Microfabricated needles for transdermal delivery of macromolecules and nanoparticles: Fabrication methods and transport studies

Devin V. McAllister*, Ping M. Wang*, Shawn P. Davis*, Jung-Hwan Park*†, Paul J. Canatella*, Mark G. Allen‡, and Mark R. Prausnitz*†§

*School of Chemical and Biomolecular Engineering, †Wallace H. Coulter Department of Biomedical Engineering, and ‡School of Electrical and Computer Engineering, Georgia Institute of Technology, Atlanta, GA 30332

Edited by Robert Langer, Massachusetts Institute of Technology, Cambridge, MA, and approved September 25, 2003 (received for review March 6, 2003)

Arrays of micrometer-scale needles could be used to deliver drugs, proteins, and particles across skin in a minimally invasive manner. We therefore developed microfabrication techniques for silicon, metal, and biodegradable polymer microneedle arrays having solid and hollow bores with tapered and beveled tips and feature sizes from 1 to 1,000 μm. When solid microneedles were used, skin permeability was increased *in vitro* by orders of magnitude for macromolecules and particles up to 50 nm in radius. Intracellular delivery of molecules into viable cells was also achieved with high efficiency. Hollow microneedles permitted flow of microliter quantities into skin *in vivo*, including microinjection of insulin to reduce blood glucose levels in diabetic rats.

transdermal drug delivery | skin | microelectromechanical systems | solid microneedle | hollow needle injection

Hypodermic needles have provided the gold standard for drug delivery for over a century, but advances in biotechnology make their limitations increasingly apparent. As devices that transport molecules of nanometer dimensions, the millimeter and larger length scales of conventional needles are often unnecessary, and they cause pain and limit targeted delivery. We therefore sought to test the hypothesis that needles of micrometer dimensions can create transport pathways large enough for small drugs, macromolecules, nanoparticles, and fluid flow, but small enough to avoid pain and facilitate highly localized and even intracellular targeting.

The microelectronics revolution has provided tools for highly precise, reproducible, and scalable methods to fabricate structures of micrometer dimensions (1). This lithography-based approach can produce large arrays of microneedles that can be inserted into cells, skin, or other tissues. The increased importance of macromolecular therapeutics, combined with the newly acquired power of microfabrication, has recently prompted interest in fabricating (2–6) and testing (7, 8) microneedles for drug delivery.

In this study, we describe fabrication techniques used to make needles out of silicon, metal, polymer, and glass that have a range of geometries, can produce needles ranging from in-plane to normally protruding from substrates, and can be formed in large two-dimensional arrays. These methods mostly require just one or two fabrication steps or a single molding step and use technologies that are readily scalable for inexpensive mass production. We also demonstrate the ability of these microneedles to deliver molecules into cells and skin by using cell culture, cadaver skin, and hairless rats.

Methods

Fabrication of Silicon Microneedles. Solid microneedles were etched from silicon substrates as described previously (9). Briefly, chromium was sputter deposited and then lithographically patterned (e.g., 20 × 20 arrays of 80-μm-diameter dots with 150-μm center-to-center spacing) onto 2-inch (5-cm), ⟨100⟩ oriented silicon wafers. Reactive ion etching (RIE; Plasma Therm, St. Petersburg, FL) was then carried out with 20 standard cm^3/min (sccm) SF_6 and 15 sccm O_2 at a pressure of 20 Pa and power of 150 W for a run time of ≈200 min. Microneedle fabrication was finished when the chromium masks became fully undercut and fell off the needle tips.

To form the bores of hollow microneedles, polymer photoresist was spin-coated and then lithographically patterned (e.g., 10 × 10 arrays of 60-μm-diameter holes with 300-μm center-to-center spacing) onto 2-inch, ⟨100⟩ oriented silicon wafers (26). Inductively coupled plasma reactive ion etching (ICP-RIE; Plasma Therm) was then carried out by using a modified Bosch process (10) to yield straight-walled holes completely through the 350-μm-thick wafer. With the addition of a lithographic alignment step, microneedles were etched around the holes as for solid silicon needles.

Fabrication of Microneedle Masters. To serve as masters for subsequent fabrication of micromolds, microneedle structures were etched into silicon and polymer substrates (27). To make molds for symmetrically tapered needles, the solid silicon microneedles described above were used as masters. To prepare asymmetrically beveled microneedle masters, cylinders of SU-8 epoxy photoresist (MicroChem, Newton, MA) were lithographically defined (e.g., 50-μm radius, 250–600 μm tall, and 600–1,500 μm center-to-center spacing) on top of 2-inch silicon wafers; the spaces between cylinders were filled with melted polylactic-*co*-glycolic acid (PLGA; Birmingham Polymers, Birmingham, AL). The surface was then coated with Al or Cu by electron beam deposition and lithographically patterned as 900 × 9,000 μm rectangular masks asymmetrically positioned with multiple cylinders located under the wide edge of each mask. As described above for silicon needle fabrication, RIE was carried out such that underetch beneath the masks occurred, which provided a beveled shape at the top of each cylinder. After the remaining PLGA was removed with methylene chloride, these masters were used to make polymer micromolds.

Fabrication of Microneedle Molds. Silicon, metal, and polymer micromolds were made for subsequent fabrication of metal and polymer needles (11).

Silicon micromolds. Silicon molds were made by directly etching arrays of cylindrical holes through the entire thickness of a silicon wafer by using inductively coupled plasma RIE, as described above, to generate hollow lumens for silicon microneedles. These molds were used to fabricate hollow straight-walled microneedles out of metal.

This paper was submitted directly (Track II) to the PNAS office.

Abbreviations: RIE, reactive ion etching; PDMS, polydimethylsiloxane.

§To whom correspondence should be addressed. E-mail: mark.prausnitz@chbe.gatech.edu.

Metal micromolds. Metal micromolds were fabricated by electroplating NiFe onto solid silicon microneedle masters. After depositing a seed layer of Ti/Cu and covering the back side of the array with Scotch tape (3M, Minneapolis) to protect it from being electroplated, we placed the needle master in a NiFe plating bath (200 g/liter $NiSO_4 \cdot H_2O$, 5 g/liter $NiCl_2 \cdot H_2O$, 3 g/liter saccharin, 8 g/liter $FeSO_4 \cdot H_2O$, 25 g/liter H_3BO_3). Plating for 6 h at 10–20 mA/cm^2 provided a 50- to 100-μm coating of NiFe. Complete removal of the silicon master by reactive ion etching (as above) yielded a NiFe micromold suitable for making solid polymer needles by injection molding.

Polymer micromolds for solid needles. Polymer micromolds were fabricated by a number of different methods. In one approach, polydimethylsiloxane (PDMS) micromolds were fabricated from silicon or polymer masters. A mold was formed by coating a microneedle master with silicone oil (DC 200, Fluka), pouring a layer of PDMS (Sylgard 184, Dow Corning, Midland, MI) up to 8 mm thick onto the master, applying vacuum to remove any entrapped air bubbles, curing at 90°C for 1 h, cooling, and gently peeling off the mold (which left the master intact for reuse). These molds were used to fabricate solid microneedles from both metal and polymer.

Another approach involved spin casting SU-8 epoxy onto a glass slide at a thickness that was ≈50 μm taller than the height of the microneedle master. After inserting the master into the epoxy, the epoxy was cured by baking on a hotplate (LHS-721P, Omega, Stamford, CT) and exposure to UV light (≈5,000 mJ; model 1100 aligner, Optical Associates, Milpitas, CA). Complete removal of the silicon master by RIE (as above) yielded a polymer mold suitable to make solid metal microneedles by electroplating.

Polymer micromolds for hollow needles. To make molds for hollow metal microneedles based on silicon masters, SU-8 epoxy was spun on at a thickness slightly taller than the microneedle master, cured by baking and exposure to UV light, and then etched back in an O_2/CHF_3 plasma RIE to expose the tips of the silicon microneedle master (e.g., upper 5–10 μm). The samples were then flipped over and etched by SF_6 plasma RIE to remove all of the silicon. The resulting polymer mold had conical holes bored completely through, suitable to make hollow metal microneedles by electroplating.

Molds for hollow metal microneedles were also made without the need for microneedle masters (26). Straight-walled molds were made by spin coating SU-8 epoxy onto a silicon wafer or glass slide coated with a 100-nm layer of titanium. After soft baking, an array of holes was lithographically patterned into the epoxy, which was then baked after exposure and developed in trichloroethylene. The mold was separated from the substrate by etching the titanium layer with hydrofluoric acid (5%), which yielded a polymer mold with cylindrical holes bored completely through, suitable for electroplating hollow metal microneedles with straight walls.

To fabricate hollow metal microneedles with tapered walls without the need for masters, polymer molds were formed by drilling holes of the desired geometry into polyimide (Kapton HN, DuPont, Circleville, OH) or polyethylene terephthalate (Mylar, DuPont, Wilmington, DE) sheets by using an excimer laser (Micromaster, Resonetics, Nashua, NH) (28). This method yielded tapered holes bored completely through, which were used for electroplating hollow metal microneedles with tapered walls.

Fabrication of Metal Microneedles. Metal microneedles were fabricated by electrodeposition onto polymer or silicon micromolds sputter coated with a Ti/Cu seed layer (28). On hollow microneedle molds, the outer surface of the mold adjacent to the needle tips was covered with powder coating tape (Shercon, Santa Fe Springs, CA) to protect it from being electroplated. A Ni or NiFe bath was used at a current density of 10 mA/cm^2 to deposit a 5- to 50-μm-thick layer of metal to form the microneedle walls of hollow microneedles. To make solid microneedles, plating was continued until the molds were filled. Although PDMS molds could be gentled peeled off the resulting needles, molds made of polyimide and polyethylene terephthalate were removed in an alkaline bath (1 M NaOH, boiling), silicon was removed in a 20% KOH bath, and SU-8 was removed with an O_2/CHF_3 plasma (RIE).

Fabrication of Polymer Microneedles. Polymer microneedles were made by melting polyglycolic acid (inherent viscosity = 1.71 dl/g; Birmingham Polymers), polylactic acid (1.48 dl/g; Alkermes, Cincinnati, OH) or polylactic-*co*-glycolic acid (50/50; 0.49 dl/g; Birmingham Polymers) into PDMS micromolds at 120–250°C, applying vacuum, and peeling the molds off (11).

Fabrication of Glass Microneedles. Glass microneedles were made by using conventional drawn-glass micropipette techniques (12). Glass capillaries (o.d. 1.5 mm, i.d. 1.1 mm, B150-110-10, borosilicate glass, Sutter Instruments, Novato, CA) were pulled in a micropipette puller (P-97, Sutter Instruments) and then beveled (BV-10, Sutter Instruments).

Cell Culture Studies. DU145 cells (American Type Culture Collection) were cultured as monolayers in 100 × 15 mm sterile polystyrene Petri dishes (Fisher Scientific) by using RPMI 1640 growth medium (Mediatech, Herndon, VA) supplemented with 10% (vol/vol) FBS (Mediatech), 100 units/ml penicillin, 100 μg/ml streptomycin, and 250 μg/ml amphotericin B (Sigma). Cell cultures were incubated at 37°C and 95% relative humidity in a 5% CO_2/95% air atmosphere until they formed a confluent monolayer.

After decanting the cell growth medium, 10^{-4} M calcein (Molecular Probes) in PBS (Sigma) was added to the Petri dish. An array of microneedles was pressed with a force of 10 g into a portion of the monolayer and removed after 5 s. Two minutes later, the calcein solution was decanted and the cells were washed three times with PBS. Finally, a solution of 10 μg/ml propidium iodide (Molecular Probes) was added to stain nonviable cells. Intracellular uptake of calcein (green fluorescence) and loss of viability indicated by propidium iodide staining (red fluorescence) were determined by imaging monolayers by using fluorescent microscopy (Olympus).

***In Vitro* Transdermal Transport Studies.** Rates of transdermal transport were determined by piercing human cadaver epidermis with microneedles. Skin was obtained from the abdomen or back of human cadavers (Emory University Body Donor Program, Atlanta) with approval of the Georgia Tech and Emory University Institutional Review Boards. Epidermis was isolated by incubating in 60°C water for 2 min and gently removing epidermis. Because the primary barrier to transdermal transport is the stratum corneum (the upper 10–15 μm of the epidermis), the use of epidermis rather than full-thickness skin is a well established model for transdermal drug delivery (13). The term "transdermal" delivery is typically used to refer to transport across epidermis to the capillaries below the dermal–epidermal junction (for systemic administration) and does not usually refer to transport across the dermis. Mathematical modeling (not shown) suggested that removing the diffusional barrier of dermis above these capillaries may overestimate skin permeability by up to a factor of 2 for our microneedle data. However, using full-thickness skin could underestimate permeability by a factor of 5 because of the presence of excess dermis.

Epidermis mounted in Franz diffusion chambers at 37°C was bathed in the receiver compartment (lower, viable epidermis side) with PBS and in the donor compartment (upper, stratum corneum side) with 1 mM calcein (Sigma), 100 units/ml insulin (Humulin-R,

Eli Lilly), 80 μM Texas red-labeled BSA (Molecular Probes), or polystyrene latex nanospheres at concentrations of 2.5×10^{14} nanospheres per ml (25-nm radius) and 2.4×10^{13} nanospheres per ml (50-nm radius) (Polysciences, Warrington, PA). To prevent insulin aggregation, 10 mM *n*-octyl β-D-glucopyranoside (Sigma) was added to donor and receiver solutions when insulin was present. Skin permeability was determined by measuring solute concentrations in the receiver compartment over time by calibrated spectrofluorimetry (calcein, BSA, and nanospheres) or RIA (insulin; Linco Research, St. Charles, MO). Skin was temporarily removed from the diffusion chamber and placed on a supported surface whenever microneedles were inserted.

Epidermis samples with arrays of microneedles either inserted or inserted and then removed were chemically fixed with formalin and then freeze dried after dehydration using graded ethanol substitution. Gold-coated samples were examined by scanning electron microscopy.

***In Vivo* Microinjection Studies.** The ability of microneedles to inject compounds into skin was assessed in diabetic, hairless rats by using a protocol approved by the Georgia Tech Institutional Animal Care and Use Committee. Hairless rats (healthy, male, adult, 300–400 g, Charles River Breeding Laboratories) were injected i.v. with 100 mg/kg streptozotocin (Sigma) in a volume of 700 μl. Over the next day, diabetes developed because of destruction of pancreatic islet cells by streptozotocin. Before microinjection studies, rats were anesthetized by i.p. injection of urethane (Sigma) and verified to have successful induction of diabetes by verifying blood glucose levels of 350–500 mg/dl.

A glass microneedle was then filled with either PBS or 100 units/ml insulin (Humulin-R) and drilled with a circular motion to a depth of 500–800 μm into the dorsal skin. A pressure of 10 psi (1 psi = 6.89 kPa) was applied for 30 min to inject fluid into the skin. Blood was collected periodically by tail vein laceration and assayed for glucose concentration (Accu-chek Compact blood glucose meter, Roche Diagnostics).

Theoretical Modeling of Transdermal Diffusion. We modeled permeability, k, of skin with holes made by microneedles by assuming that intact skin is effectively impermeable and that pathways created by microneedles are filled with water:

$$k = f\frac{D}{L}, \qquad [1]$$

where f is fractional skin area containing holes from microneedles, D is effective solute diffusivity within holes, and L is hole length [50 μm, corresponding to epidermis thickness (13)].

Hole geometry was idealized as an annulus when needles were inserted into skin and left *in situ*. When needles were inserted and then removed, holes were idealized as cylinders. Examination of skin samples by scanning electron microscopy indicated the annular gap width to be 250 $\pm$ 100 nm and cylinder diameter to be 12 $\pm$ 3 μm (data not shown). By using these measurements, f was calculated to be 7×10^{-4} with needles inserted and 5×10^{-3} after needles were removed. The value of f with needles inserted was calculated by using $f = n\pi[(R + W)^2 - R^2]/A$, where n is the number of microneedles (400), R is needle radius (10 μm), W is annular gap width (250 nm), and A is skin area under the array (9 mm^2). For needles removed, $f = n\pi r^2/A$, where r is the radius of residual holes (6 μm).

Solute diffusivity in dilute bulk solution (D_∞) was used as the effective diffusivity within cylindrical holes and was determined as follows: calcein from the Stokes–Einstein equation (14) using molecular radius of 6.5 Å (5.0×10^{-6} cm^2/s), hexameric insulin from a semiempirical correlation (15) (1.3×10^{-6} cm^2/s), and BSA from experimental measurement (16) and correcting for temperature and viscosity by using the Stokes–Einstein equation (5.9×10^{-7} cm^2/s), and nanospheres by using the Stokes–Einstein equation (1.3×10^{-7} cm^2/s and 6.5×10^{-8} cm^2/s for 25 nm and 50 nm radii, respectively). Possible hindrance to diffusion of nanospheres within annular gaps was accounted for assuming spherical particles diffusing in slits according to Eq. **2** (17).

$$\frac{D}{D_\infty} = \frac{1}{1-\lambda}\left[1 + \frac{9}{16}\lambda\ln(\lambda) - 1.19358\lambda + 0.159317\lambda^3\right], \qquad [2]$$

λ is the ratio of particle radius to slit half-width.

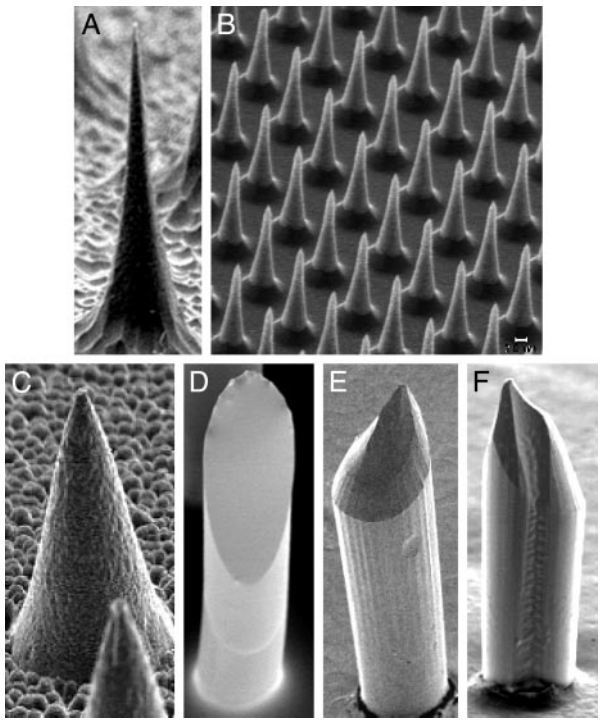

Fig. 1. Solid microneedles fabricated out of silicon, polymer, and metal, imaged by scanning electron microscopy. (*A*) Silicon microneedle (150 μm tall) from a 400-needle array etched out of a silicon substrate. (*B*) Section of an array containing 160,000 silicon microneedles (25 μm tall). (*C*) Metal microneedle (120 μm tall) from a 400-needle array made by electrodepositing onto a polymeric mold. (*D–F*) Biodegradable polymer microneedles with beveled tips from 100-needle arrays made by filling polymeric molds. (*D*) Flat-bevel tip made of polylactic acid (400 μm tall). (*E*) Curved-bevel tip made of polyglycolic acid (600 μm tall). (*F*) Curved-bevel tip with a groove etched along the full length of the needle made of polyglycolic acid (400 μm tall).

Results

Fabrication of Solid Microneedles Made of Silicon, Metal, and Polymer. Arrays of solid microneedles were fabricated either by etching into silicon or polymer substrates or by filling molds with metal or polymer (Fig. 1). Fig. 1 *A* and *B* shows solid silicon microneedles prepared in a reactive ion etcher using an optimized ratio of SF_6 to O_2 in the plasma to balance anisotropic with isotropic etching that causes "under-etch" beneath the masking material (9). The needle in Fig. 1*A* is $\approx$150 μm tall, 80 μm at its base, and tapered to a 1-μm radius tip. By altering mask size, mask-to-mask spacing, and etching chemistry, needles as long as 200 μm and as short as 25 μm (Fig. 1*B*) have been fabricated at densities from 10^3 to 10^5 needles per cm^2.

Molding techniques have also been developed to fabricate microneedle arrays. To reproduce silicon needles in other materials, polymeric and metal molds of those needles were cast and filled either with metal by electrodeposition or with polymer by

injection molding to form exact replicas. Because needle tip geometry is important for ease of insertion into tissue, various needle tip designs were etched into silicon or polymer substrates, transferred into polymeric molds, and used to prepare replicas. In contrast to the thin needle with an extremely sharp tip shown in Fig. 1*A*, Fig. 1*C* shows a metal replica with a wider geometry made of NiFe, which was fabricated by using an SU-8 polymer mold derived from a silicon master. This replica looks identical to the master from which it was copied (result not shown).

Fig. 1 *D–F* shows three different designs of beveled-tip microneedles made of biodegradable polyesters, which were fabricated by using PDMS polymer molds derived from etched SU-8 polymer masters. The beveled geometry was achieved by preferentially etching only on one side of the needle, which was accomplished by asymmetrically placing masks over the polymer posts that were substrates for the needle masters (see *Methods*). Fig. 1*F* additionally has a groove etched along the full length of the needle created by using a notch in the lithographic mask. These molds can be used repeatedly; we have made more than 100 replicate needle arrays from individual molds. The resulting needles are sharp and strong enough to repeatedly insert into human skin *in vivo* without breaking.

Fabrication of Hollow Microneedles Made of Silicon, Metal, and Glass. Hollow microneedle arrays have also been made by direct etching and molding. Hollow silicon microneedles were fabricated by first etching holes although silicon wafers by deep RIE and then etching microneedles around the holes, as described above. In this case, the bore diameter was constant (e.g., 60 μm) and the wall thickness increased toward the needle base. Hollow metal microneedles were made by forming polymer or silicon molds and electrodepositing nickel, gold, or other metals onto the mold (Fig. 2). Such needles have a constant wall thickness (e.g., 10 μm) and a bore that widens toward the needle base. Hollow microneedles have been fabricated with widths between 35 and 300 μm and lengths between 150 and 1,000 μm. Although weaker than solid needles, these hollow microneedles are sufficiently strong to repeatedly insert into human skin *in vivo* with forces often much smaller than forces that caused needle fracture (data not shown).

Fabrication of hollow microneedles with straight walls (i.e., that do not taper) was achieved by using molds with cylindrical holes created either by deep RIE through silicon wafers or lithographically defining holes in SU-8 photoresist polymer. A thin coating of metal was then electrodeposited onto the molds to produce needles such as shown in Fig. 2*A*. Tapered hollow needles were fabricated either by making a mold from a silicon master (e.g., Fig. 1*A*) or laser drilling tapered holes into polymer sheets, followed by electrodeposition of a thin metal coating onto the mold (Fig. 2 *C* and *D*). Tapered glass microneedles were also made by using conventional micropipette pulling techniques (Fig. 2*B*).

Transdermal Transport Facilitated by Solid Microneedles. Microneedles were designed for insertion into human skin for painless transdermal drug delivery. Because skin's outer stratum corneum provides the primary permeability barrier, microneedles need only pierce past this 10- to 15-μm-thick layer to administer drugs that can diffuse through highly permeable viable epidermis to capillaries found in the superficial dermis below (18). Because there are no nerves in the stratum corneum, such short needles might not stimulate pain. To account for hairs, dermatoglyphics (i.e., tiny wrinkles), and other surface features, as well as local deformation of the skin when pressed with microneedles, 150-μm tall microneedles were used (Fig. 1*A*).

To assess the ability of microneedles to create transport pathways across stratum corneum, an array of 400 solid silicon needles in an area of 9 mm^2 was pressed into human cadaver epidermis and then removed. Cadaver epidermis is widely used

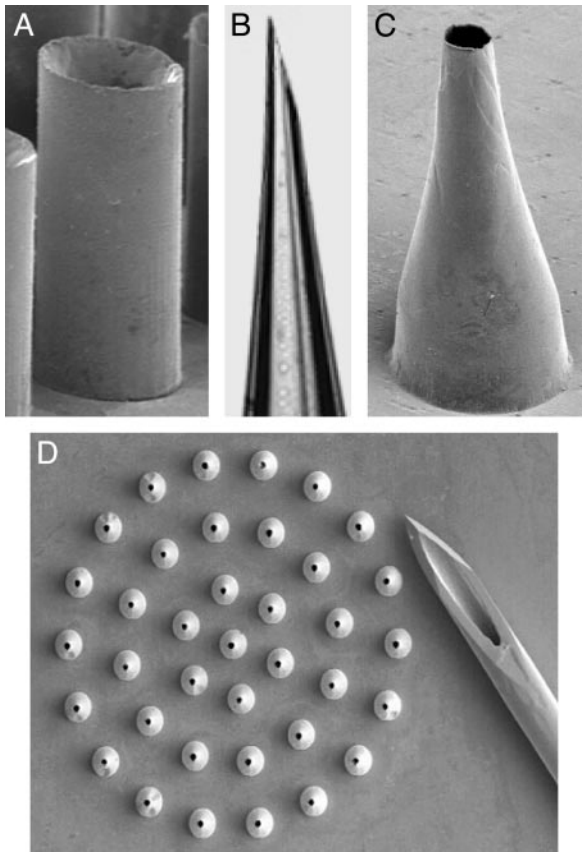

Fig. 2. Hollow microneedles fabricated out of silicon, metal, and glass imaged by optical and scanning electron microscopy. (*A*) Straight-walled metal microneedle from a 100-needle array fabricated by electrodeposition onto a polymer mold (200 μm tall). (*B*) Tip of a tapered, beveled, glass microneedle made by conventional micropipette puller (900-μm length shown). (*C*) Tapered, metal microneedle (500 μm tall) from a 37-needle array made by electrodeposition onto a polymeric mold. (*D*) Array of tapered metal microneedles (500 μm height) shown next to the tip of a 26-gauge hypodermic needle.

to model the transport properties of human skin (13). A solution of trypan blue dye was briefly placed on the stratum corneum side and then rinsed away. Fig. 3*A* shows an image of the underside (viable epidermis) of the tissue. The array of blue spots in the shape of the microneedle array indicates that the dye rapidly diffused across the epidermis through holes made by microneedles.

Additional experiments were performed with a number of different compounds to determine skin permeability quantitatively by using Franz diffusion chambers *in vitro* (Fig. 4). In one set of experiments, arrays of microneedles were inserted and left in the skin. In this case, molecules could potentially diffuse through the gaps between microneedles and surrounding tissue. Skin permeability to calcein, insulin, and BSA was increased by orders of magnitude. This result is significant, because skin is generally considered impermeable to macromolecules (13, 19).

In a second set of experiments, arrays of microneedles were inserted and then removed from the skin, after which skin permeability was determined (Fig. 4). In this case, compounds could diffuse through residual holes left in the skin. Skin permeability to calcein, insulin, and BSA was increased by an additional order of magnitude above the "needles inserted" case. Moreover, significant numbers of latex nanoparticles were detected crossing the skin, which suggests the possibility of using microneedles to deliver controlled-release particles or virus-based vaccines.

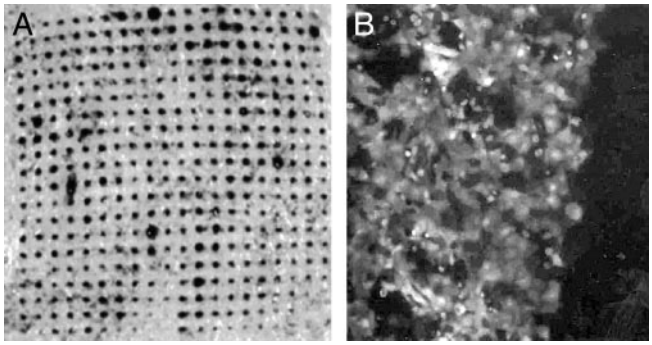

Fig. 3. Optical micrographs showing molecular transport induced by microneedles. (*A*) An array of microneedles (Fig. 1*A*) was inserted and removed from human cadaver skin, which was subsequently exposed to trypan blue on the exterior stratum corneum side. The array of dark dots shown on the interior viable epidermis side indicates that microneedles created transport pathways across the tissue. (*B*) An array of 25-μm-tall microneedles (Fig. 1*B*) was briefly inserted into a monolayer of prostate cancer cells bathed in a solution of calcein, a cell-impermeant fluorescent tracer. Cells on the left were treated with microneedles and show bright fluorescence, indicating uptake of calcein. Cells on the right (dark area) were not treated with microneedles and show little fluorescence, indicating little or no uptake. Most cells remained viable after treatment (data not shown).

To understand the mechanism by which microneedles increase skin permeability, we theoretically modeled transdermal transport as diffusion through holes of known geometry made by insertion of microneedles. Predictions using this model, which requires no adjustable parameters, are shown in Fig. 4 to agree with the data. Model predictions are within the 95% confidence interval of each experimental data point, which supports the interpretation that transport occurred by diffusion through water-filled holes across the skin.

To put these results into better perspective, a 1-cm^2 patch of microneedles containing insulin in a conventional formulation of 100 units/ml is expected to deliver on the order of 1 unit/h insulin (see Fig. 4), which is sufficient to meet the basal needs of many diabetics (20). A representative meal-time need of 10 units

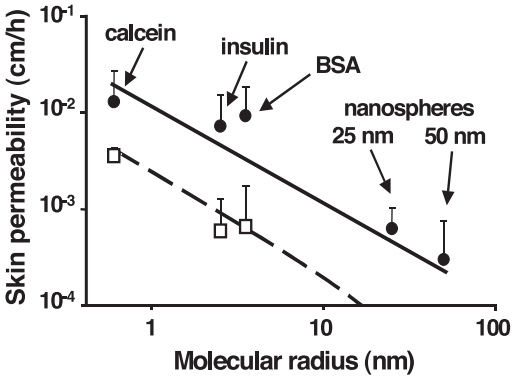

Fig. 4. Skin permeability to molecules and particles of different sizes after treatment with microneedles. The permeability of human cadaver epidermis was increased by orders of magnitude with a 400-needle array (Fig. 1*A*) inserted (□) and after the array was removed (●) for calcein, insulin, BSA, and latex nanospheres of 25 nm and 50 nm radius. Permeability to nanospheres with needles inserted was below the detection limit, on the order of 10^{-4} cm/h. In the absence of microneedles, permeability to all compounds was below their detection limits, on the order of 10^{-6} to 10^{-4} cm/h (data not shown). Mean values ± SEM are shown for at least six replicates. Predictions are shown for needles inserted (dashed line) and needles removed (solid line) by using a model requiring no adjustable parameters (Eq. **1** coupled with the Stokes–Einstein equation to interrelate molecular radius and diffusivity).

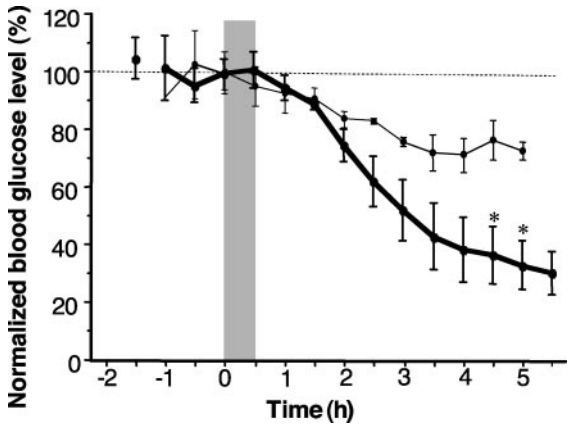

Fig. 5. Blood glucose levels in diabetic hairless rats shown as a function of time after injection of insulin solution at 10 psi (●) (n = 3, 4.3 ± 0.7 μl delivered) or 14 psi (○) (n = 4, 28 ± 11 μl delivered). Blood glucose level was measured before and after insulin was microinjected through a hollow, glass microneedle inserted into rat skin for 30 min (shaded region). Each data point represents the mean (±SEM) of three or four measurements on different rats.

typically absorbed on the time scale of an hour or more from a conventional rapid-acting injection could be addressed by using a 2-cm^2 patch supplied by a commercially available 500 units/ml insulin formulation.

Insulin Microinjection to Diabetic Rats. To facilitate delivery into skin by convection, hollow microneedles were used to inject insulin and other solutions into the skin of hairless rats *in vivo*. When a single glass microneedle (e.g., Fig. 2*B*) was inserted into the skin for 30 min, up to 32 μl of fluid could be flowed into the skin at a pressure of 10 psi (data not shown). Smaller amounts could be injected by using lower pressures or shorter periods of time with no apparent lag time. Additional microscopy studies demonstrated intradermal and intraepidermal microinjection of low molecular weight dyes, as well as 2.8-μm fluorescence-labeled latex particles (data not shown).

To test the ability of microneedles to deliver a biologically active agent *in vivo*, microinjection of insulin was studied in diabetic hairless rats. As shown in Fig. 5, a 30-min microinfusion of insulin at 10 or 14 psi caused a steady reduction in blood glucose level over a 5-h period, which corresponded to a drop of up to 70% from preinfusion levels (340–470 mg/dl). This level was statistically different from controls ($P < 0.05$), where neither infusion of saline nor placement of insulin solution on the skin without microneedles changed blood glucose levels ($P > 0.05$, data not shown). A dose-dependent response was observed, where infusion at larger pressure caused a larger drop in blood glucose ($P < 0.05$ for >4 h). Subcutaneous injection of 0.05 and 0.5 unit of insulin bracketed the response seen when microneedles were used (data not shown).

Intracellular Delivery Using Solid Microneedles. Many laboratory applications require delivery of molecules into cells, for example, to alter cell function. To determine the ability of microneedles to insert into cell membranes and thereby introduce exogenous molecules into large numbers of viable cells, we bathed a monolayer of human prostate cancer cells in a solution of calcein (an inert cell-impermeant fluorescent molecule) and briefly pressed an array of solid microneedles into the cells (Fig. 1*B*). As designed for this application, these needles were 25 μm tall, which is comparable to the height of a confluent DU145 cell monolayer; measured 15 μm at their base and less than 1 μm at their tip, which facilitated easy insertion; were spaced 25 μm

ENGINEERING

apart, which is similar to the cell-to-cell spacing in a confluent monolayer; and numbered 160,000 needles per cm^2.

After the needles had been removed and the extracellular calcein had been washed away, ≈85% of cells beneath the array contained bright green fluorescence (left side of Fig. 3*B*), indicating substantial uptake of the marker compound. Control cells in the same monolayer that were not pierced by microneedles showed minimal green fluorescence (right side of Fig. 3*B*). Subsequent exposure to a red viability stain indicated that ≈90% of cells were viable (data not shown). This result demonstrates that micrometer-scale piercing of cells can induce molecular uptake while maintaining high cell viability, in agreement with previous observations (21, 22).

Discussion

Possible Uses of Microneedles. Microneedles sit at the interface between transdermal patches and hypodermic needles, attempting to gain the advantages and eliminate the disadvantages of each. Hypodermic needles effectively deliver almost any drug at almost any rate across the skin but are limited by pain, need for medical expertise, and difficulty to have controlled delivery over long periods of time. In contrast, transdermal patches largely eliminate these limitations, but suffer from an inability to deliver most drugs across skin at useful rates. We have hypothesized that microneedles may be small enough to capture the convenience of patches but large enough to create micrometer-scale pathways across the skin for drug delivery. Previous studies have shown that microneedles can be painlessly inserted into the skin of human subjects (23). Additional studies will be needed to further establish the ease and efficacy of microneedle-based delivery in a clinical environment.

We envision using solid microneedles in combination with current transdermal patch technology. Integrated into a patch, microneedles may provide a minimally invasive method to increase skin permeability for diffusion-based transport that could make transdermal delivery of many drugs possible, including large molecules such as proteins. Hollow microneedles, either as individual needles or as multineedle arrays, might be used for convection-based delivery. This microinfusion approach could increase rates of delivery beyond those of passive patches and permit rates to be modulated in real time by a microprocessor-controlled pump, which could include a user interface for input by patients or healthcare providers.

Advantages of Metal and Polymer Microneedles. Although silicon needle arrays (e.g., Fig. 1 *A* and *B*) can be fabricated in cleanroom facilities in widespread use in the microelectronics industry, the metal and polymer needles shown in Fig. 1 *C–E* and Fig. 2 offer a number of practical advantages. First, fabrication of metal and polymer microneedles should be less expensive and readily scalable to mass production because: (*i*) metal and polymer raw materials are widely available and generally less expensive than silicon wafers, (*ii*) the electroplating and polymer molding techniques used to make these needles can be set up in a conventional manufacturing environment without the need for cleanroom facilities, and (*iii*) the fabrication techniques we developed involve relatively simple single-step molding operations, which contrasts with most other published methods that require more complex multistep fabrication schemes (24).

Regarding microneedle safety, many metal and polymer materials have established safety records in medical devices (25), whereas silicon is a new and relatively untested biomaterial. In contrast to our previous observations of occasional breakage of silicon microneedle tips upon insertion into skin (9), our polymer and metal microneedles are stronger (data not shown). As an added safety measure, polymer microneedles were fabricated by using biodegradable materials, which suggests that if such a microneedle accidentally broke off in the skin, it would safely degrade and disappear over time.

Conclusions

In conclusion, practical microfabrication techniques were developed to yield silicon, metal, and polymer microneedles of micrometer dimensions in various geometries. Solid microneedles were shown to pierce skin and thereby increase skin permeability by orders of magnitude to levels that may permit clinical delivery of macromolecules across skin. Solid needles also permeabilized cell membranes for intracellular delivery of marker compounds. Hollow microneedles were shown to microinject insulin to modulate blood glucose levels in diabetic rats. Together, these results suggest that microneedles are a useful approach to transdermal drug delivery.

We thank D. Ackley, S. Henry, W. Martanto, J. Mayberry, and P. Patel for helpful discussions and assistance in the laboratory. This work was supported in part by the American Diabetes Association, the Defense Advanced Research Planning Agency, the National Science Foundation, and the National Institutes of Health.

1. Madou, M. (1997) *Fundamentals of Microfabrication* (CRC, Boca Raton, FL).
2. Chen, J. & Wise, K. D. (1997) *IEEE Trans. Biomed. Eng.* **44,** 760–769.
3. Brazzle, J., Papautsky, I. & Frazier, A. B. (1999) *IEEE Eng. Med. Biol. Mag.* **18,** 53–58.
4. Lin, L. & Pisano, A. P. (1999) *IEEE J. Micromech. Syst.* **8,** 78–84.
5. Stoeber, B. & Liepmann, D. (2000) *Proc. ASME MEMS Dev. 2000 IMECE* **2,** 355–359.
6. Griss, P., Enoksson, P., Tolvanen-Laakso, H. K., Merilainen, P., Ollmar, S. & Stemme, G. (2001) *J. Microelectromech. Syst.* **10,** 10–16.
7. Matriano, J. A., Cormier, M., Johnson, J., Young, W. A., Buttery, M., Nyam, K. & Daddona, P. E. (2002) *Pharm. Res.* **19,** 63–70.
8. Mikszta, J. A., Alarcon, J. B., Brittingham, J. M., Sutter, D. E., Pettis, R. J. & Harvey, N. G. (2002) *Nat. Med.* **8,** 415–419.
9. Henry, S., McAllister, D., Allen, M. G. & Prausnitz, M. R. (1998) *J. Pharm. Sci.* **87,** 922–925.
10. Laermer, F. & Schilp, A. (1996) U.S. Patent 5,501, 893.
11. McAllister, D. V. (2000) Ph.D. thesis (Georgia Institute of Technology, Atlanta).
12. Brown, K. T. & Flaming, D. G. (1986) *Advanced Micropipette Techniques for Cell Physiology* (Wiley, New York).
13. Bronaugh, R. L. & Maibach, H. I., eds. (1999) *Percutaneous Absorption: Drugs-Cosmetics-Mechanisms-Methodology* (Dekker, New York).
14. Poling, B. E., Prausnitz, J. M. & O'Connell, J. P. (2001) *The Properties of Gases and Liquids* (McGraw-Hill, New York).
15. Polson, A. J. (1950) *J. Phys. Colloid Chem.* **54,** 649–652.
16. Tyn, M. T. & Gusek, T. W. (1990) *Biotechnol. Bioeng.* **35,** 327–338.
17. Panwar, Y. & Anderson, J. L. (1993) *Ind. Eng. Chem. Res.* **32,** 743–746.
18. Champion, R. H., Burton, J. L. & Ebling, F. J. G., eds. (1992) *Textbook of Dermatology* (Blackwell Scientific, London).
19. Amsden, B. G. & Goosen, M. F. A. (1995) *AIChE J.* **41,** 1972–1997.
20. Davidson, M. B. (1998) *Diabetes Mellitus: Diagnosis and Treatment* (Saunders, Philadelphia).
21. Hashmi, S., Ling, P., Hashmi, G., Reed, M., Gaugler, R. & Trimmer, W. (1995) *BioTechniques* **19,** 766–770.
22. Chun, K., Hashiguchi, G., Toshiyoshi, H. & Fujita, H. (1999) *Jpn. J. Appl. Phys. Part 2* **38,** 279–281.
23. Kaushik, S., Hord, A. H., Denson, D. D., McAllister, D. V., Smitra, S., Allen, M. G. & Prausnitz, M. R. (2001) *Anesth. Analg.* **92,** 502–504.
24. McAllister, D. V., Allen, M. G. & Prausnitz, M. R. (2000) *Annu. Rev. Biomed. Eng.* **2,** 289–313.
25. Ratner, B. D., Hoffman, A. S., Schoen, F. J. & Lomons, J. E., eds. (1996) *Biomaterials Science: An Introduction to Materials in Medicine* (Academic, San Diego).
26. McAllister, D. V., Cros, F., Davis, S. P., Latta, L. M., Prausnitz, M. R. & Allen, M. G. (2000) in *Transducers '99: 10th International Conference on Solid-State Sensors and Actuators* (Elsevier, Lausanne, Switzerland), pp. 1098–1101.
27. Park, J. H., Davis, S. P., Yoon, Y. K., Prausnitz, M. R. & Allen, M. G. (2003) in *The 16th Annual International Conference on Micro Electro Mechanical Systems* (IEEE, Piscataway, NJ), pp. 371–374.
28. Davis, S. P., Prausnitz, M. R. & Allen, M. G. (2003) in *Transducers '03: The 12th International Conference on Solid-State Sensors, Actuators, and Microsystems* (IEEE, Piscataway, NJ), pp. 1435–1438.